Collective behavior of Zr-substituted polyoxometalates in solution: Insights from molecular dynamics simulations.

Pablo Jiménez-Lozano,[‡] Jordi Puiggalí-Jou,[‡] Alain Chaumont,[¥,] Jorge J. Carbó[‡,]**

[‡]Department de Química Física i Inorgànica, Universitat Rovira i Virgili, Tarragona 43007, Spain

[¥] Laboratoire MSM, UMR CNRS 7140, Chimie de la Matière Complexe, Université de Strasbourg, 4, rue B. Pascal, 67000 Strasbourg, France

KEYWORDS. Molecular Dynamics, polyoxometalates, zirconium, self-assembly, liquid-liquid interfaces.

ABSTRACT. The collective behavior of zirconium-substituted polyoxometallates (POMs) in aqueous solution and at the interface with organic solvents has been analyzed by means of molecular dynamics (MD) simulations with explicit solvent molecules. MD simulations using tetrabutylammonium as counterion (TBA^+) and Zr-hydroxo-aqua $[W_5O_{18}Zr(OH)(H_2O)]^{3-}$ anions (**W_5Zr**) indicate that these anions do not form permanent noncovalent contacts, but the interaction is directional occurring preferentially through Zr···Zr moiety contacts. In biphasic

chloroform/water systems, the hydrophobic TBA^+ countercations accumulate at the interface creating a positively charged layer that attracts **W_5Zr** anions. At the layer of TBAs, the **W_5Zr** anions sit with hydrophilic Zr-aqua-hydroxo moiety pointing towards the bulk aqueous solution, favoring the frequency of **W_5Zr**···**W_5Zr** and Zr···Zr contacts further increased due to the local concentration. Detailed analysis of **W_5Zr**···**W_5Zr** contacts in bulk solution revealed that interactions are driven by intercluster hydrogen-bonding between the two Zr-aqua-hydroxo moieties. Finally, potential of mean force (PMF) simulations are performed to evaluate the free-energy change when two **W_5Zr** anions approach each other in solution, showing that the free-energy penalty is low (2-3 kcal·mol^{-1}) and can be easily overcome at ambient temperature.

INTRODUCTION

POMs are polynuclear metal-oxide clusters built up from early transition metal atoms such as W, Mo or V in their highest oxidation state. They have the ability to incorporate other transition metal (TM) ions, acting as inorganic chelating ligands.[1] Thus, the combination of lacunary POMs with TM based salts leads to the formation of TM-substituted POMs, conferring them a broad range of potential applications in areas such as catalysis, material science and biotechnology. Specifically, Zr-substituted POMs have shown potential applications as structural models of catalysts for industrial oxidation processes, and as artificial metalloenzymes for biotechnological applications.[2] They were used as tractable and soluble molecular analogues of heterogeneous Zr-supported tungsten catalysts, [3] mesoporous Zr silicates, [4] or Zr-containing metal−organic frameworks (MOFs) [5] in the oxidation of organic substrates. This chemistry is influenced by the condensation of POM structures to form dimeric and other oligomeric units via inter-cluster linking. In addition, the water-stability and solubility of Zr-substituted POMs, in combination with

the Lewis acidity of Zr metal, have prompted their use as artificial metalloproteases and nucleases, showing activity in the hydrolysis of peptides and proteins, or DNA and its model systems. [6] Some of us and others have characterized the reaction mechanism for the oxidation and hydrolysis processes mentioned above.[5,7,8] However, gaining knowledge of collective behavior of Zr-substituted POMs in solution at atomistic level is of great importance and would contribute to complete the understanding of their chemistry. Moreover, most of atomistic simulations analyzed the collective behavior of plenary POMs in solution, [9-19] while the effect of the substituted TM fragment has been somewhat overlooked.[20, 21] Figure 1 shows the structure of Zr-substituted Lindqvist anion $[W_5O_{18}Zr(OH)(H_2O)]^{3-}$, which will be used in the present study (see below).

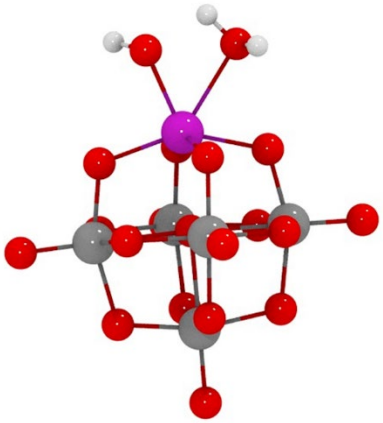

Figure 1. 3D-representation of the computed structure of $[W_5O_{18}Zr(OH)(H_2O)]^{3-}$ (**W_5Zr**) Color code: W, gray; O, red; Zr, magenta; H, white.

Nowadays, the behavior of polyoxometalate anions in solution is rationalized by their (super)chaotropic character.[22] Chaotropic anions are typically large and charge-delocalized species, resulting in a less directional ion-dipole interaction with the solvent. Consequently, they do not change the bulk water structure in large extent, reducing the desolvation energies and

favoring the assembly to biomolecules[23] and other organic substrates,[24] as well as, the self-assembly processes.[25] Valuable information of the behaviour of POMs in solution can be obtained from molecular dynamics simulations.[26] Among others, they have allowed to provide an atomistic description of chaotropic character of POM, where the hydrogen bonding pattern shows a less organized water structure in the first solvation shell of the POM,[18] as well as to characterize the assembly of POMs with proteins[7,8,18,27,28] and cyclodextrins.[19]

The collective behaviour and the POM···POM aggregation phenomena were initially studied for non-substituted Keggin-type anions using classical molecular dynamics (MD) simulations.[9-13] The most relevant findings related to this work can be summarized as follows: (1) the $[PW_{12}O_{40}]^{3-}$ anions form noncovalent dimers and oligomers in water via bridging hydrogen-bonded H_2O molecules;[9,13] (2) upon anion association, the computed free energy profile, using potential of mean force (PMF) simulations, is quite flat with a small energy minimum;[11,13] (3) the $[PW_{12}O_{40}]^{3-}$ anions display some affinity for aqueous interfaces with "oil", hydrophobic ionic liquids, or graphite;[10] (4) the aggregation of POMs depends on the charge, concentration and temperature.[12,13] Although early simulations on Keggin anions $[XW_{12}O_{40}]^{n-}$ ($X = P^{5+}$, Si^{4+}, Al^{3+}) indicate that the charge effect does not determine the anion-anion repulsions exclusively,[12] the MD simulations reported later[13] differ showing that the formation of aggregates is inhibited by increasing the negative charge of the POM. Probably, these discrepancies are due to the differences in the simulated conditions that can shift the weight of hydrophobic forces and interactions with counterions in the overall collective behavior. For example, some of us have shown that the addition of salts such as NaCl increases the ionic strength of the solution promoting POM agglomeration via cation-mediated interactions.[20] In the case of related polyoxovanadates (POVs), MD simulations found that in acetonitrile, agglomeration is favored for intermediated charged

species, while in water, the lowest-charged POVs with organic countercations tend to agglomerate.[16]

Using also MD simulations, Bo and Serapian have compared the aggregative behavior in aqueous solution of the plenary polyoxometalate anion $[AlW_{12}O_{40}]^{5-}$ with the corresponding monolacunary anion $[AlW_{11}O_{39}]^{9-}$, which has larger negative charge and an overall dipole moment.[14] The authors observed the formation of stable long-lived aggregates for monolacunary $[AlW_{11}O_{39}]^{9-}$ anions with Li^+ countercations, suggesting that the dipole moment is not responsible of aggregation but the large negative charge on the lacunary and the concomitant binding of Li^+ countercations that mediate aggregation. There have also been dynamic simulations of Zr-substituted polyoxometalates, $[W_5O_{18}Zr(OH)(H_2O)]^{3-}$, in aqueous solutions in the context of their interaction with proteins.[7,8,27] Interestingly, the atomistic description of POM···protein interaction shows that the oxygens of the POM framework form hydrogen bonds with positively charge and polar amino acids, while the Zr moiety points towards the solvent with the hydroxo and aqua ligands forming hydrogen bonds with the bulk water molecules. Thus, the interaction of Zr-substituted POMs with the surface of large biomolecules is directional with the Zr moiety acting as the hydrophilic side. In fact, X-ray structures obtained from the co-crystallization of HEWL protein and a Zr-substituted Keggin-type POM show the same type of directionality.[29]

In previous contributions, we used static density functional theory (DFT) calculations and Car−Parrinello MD simulations with explicit solvent molecules to study the nature of Zr-monosubstituted anions at different pH conditions,[30] and the mechanism of condensation of two monomers through the formation of the covalent M−μO−M linkages for Zr and other transition metals.[31] Depending on pH condition, the POM can form Zr-aqua, -hydroxo, and -aqua-hydroxo species, with preference for coordination numbers greater than 6.[30] Under the experimental

conditions proposed by Villanneau and co-workers,[32] namely the alkalination of Zr-triaqua $[W_5O_{18}Zr(H_2O)_3]^{2-}$, CPMD simulations indicate that the precursor for dimerization is the Zr-aqua-hydroxo species $[W_5O_{18}Zr(OH)(H_2O)]^{3-}$.[31] Using this type of species, we have performed a detailed study of the assembly mechanism of two Zr-substituted Lindqvist and Keggin anions, and other transition metal-substituted anions.[31] DFT calculations reveal that Zr-substituted POM can form hydrogen-bonded adducts through their Zr moieties, from which the dibridged $(\mu OH)_2$ linkages form with a low overall energy barrier due to the flexible coordination environment and large radius of Zr.[31] Here, we extent and complement previous studies by reporting a detailed analysis of the collective behavior in solution of Zr-substituted Lindqvist anion $[W_5O_{18}Zr(OH)(H_2O)]^{3-}$ using classical MD simulations. Current work analyzes the aggregation phenomena and noncovalent interactions of the Zr-substituted POMs and tetrabutylammonium cations (TBA^+) in aqueous solutions at three different concentrations. Also, to assess the affinity of Zr-substituted POMs for aqueous interfaces, we consider a water/chloroform (CLF) biphasic system. Finally, to gain quantitative insight into the interaction between these anions in water, we calculated the free energy profiles $\Delta G(d)$ as a function of the Zr···Zr distance via potential mean force (PMF) simulations.

METHODS

Classical molecular dynamics (MD) simulations. Classical molecular dynamics have been performed using the AMBER software,[33] in which the potential energy U is described by a sum of bond, angle and dihedral deformation energies as well as a pairwise additive 1-6-12 (electrostatic and van der Waals) interaction between non bonded atoms; see Equation (1).

$$V(r) = \sum_{bonds} K_b(b - b_0)^2 + \sum_{angles} K_\theta(\theta - \theta_0)^2 + \sum_{dihedrals} \left({V_n}/{2}\right)(1 + \cos[n\phi - \gamma])$$

$$+ \sum_{nonb\ ij} \left({A_{ij}}/{r_{ij}^{12}}\right) - \left({B_{ij}}/{r_{ij}^{6}}\right) + \left({q_i q_j}/{r_{ij}}\right) \quad [1]$$

Lorentz-Berthelot rules were used in order to construct the cross-terms in van der Waals interactions. The parameters for the Zr-substituted POMs were obtained following the procedure by Bonet-Avalos, Bo, Poblet and co-workers.[34] The set of Lennard-Jones parameters for W and O atoms of the oxide POM framework were taken from previous work,[34] whereas those for Zr stem from UFF force field,[35] those of the hydroxo group were taken from the OPLS Force Field[36] and finally, those for the aqua ligands are those of the TIP3P[37] water model. Atomic charges were determined by a single-point calculation performed on the optimized structure of $[W_5O_{18}Zr(OH)(H_2O)]^{3-}$ to compute the CHELPG charges derived from the electrostatic potential, using the same theory level described above.[34] Parameters for TBA^+ are the same as in our previous study on POM at interfaces.[10] Bulk water was represented with the TIP3P model,[37] while we used the Chang & Dang model for chloroform.[38] Table 1 summarizes the composition of each of the simulated systems. The POM concentration in system **A** is similar to that employed by Villanneau and co-workers[3a] in the synthesis and characterization of $[\{W_5O_{18}Zr(\mu\text{-}OH)\}_2]^{6-}$ dimer in aqueous solution (0.024 vs. 0.022 M). Then, the concentration of POM is systematically increased (systems **B** and **C**) to values close to previous MD studies[12,13] in order to evaluate the relevance of this macroscopic effect and to further characterize the POM···POM contact modes.

Table 1. Definition of the simulated systems.

Systems	**Species**	**N_{H2O}**	**Box size (Å^3)**	**[POM] (M)**
A	2 W_5Zr, 6 TBA^+	4429	51.83	0.024
B	6 W_5Zr, 18 TBA^+	4429	52.63	0.068
C	18 W_5Zr, 54 TBA^+	4429	55.13	0.178
Systems	**Species**	**N_{CLF}**	**N_{H2O}**	**Box dimension (Å)**
A'	2 W_5Zr, 6 TBA^+	991	4364	42.5 x 42.5 x 150.1
B'	6 W_5Zr, 18 TBA^+	991	4364	42.5 x 42.9 x 151.2
C'	18 W_5Zr, 54 TBA^+	991	4364	44.3 x 44.3 x 152.6

The 1-4 van der Waals and 1-4 coulombic interactions were scaled down by 2.0. All the simulations were simulated using 3D-periodic boundary conditions and an atom-based cutoff of 12 Å for noncovalent interactions. Long-range electrostatic were computed by using particle-particle mesh Ewald (PME) summation method.[39] The MD simulations were performed at 300 K starting with random velocities. The temperature was monitored by coupling the system to a thermal bath using the Berendsen algorithm[40] with a relaxation time of 0.2 ps. In the NPT simulations, the pressure was similarly coupled to a barostat with a relaxation time of 0.2 ps. All bonds involving hydrogen atoms were constrained using the SHAKE algorithm. A time step of 2 fs was used to integrate the equation of motion via the Verlet leapfrog algorithm.[41] After 500 steps of energy minimization, 0.25 ns of dynamics were performed with fix solutes (BELLY option of AMBER)[33] in order to allow the solvent to somewhat relax around the solute. This was then

followed by 0.25 ns of dynamics at constant volume (NVT) and 0.5 ns at constant pressure (NPT) of 1 atm. A 100 ns MD simulations in the NVT ensemble was then further performed to fully equilibrate the system. Finally, a production run of 500 ns at constant volume was performed using the pmemd.cuda code of the AMBER software suite. A data set of the molecular dynamics simulations in systems **A**, **B**, **C**, **A'**, **B'** and **C'** (Table 1) is available in the Zenodo repository and can be accessed via the following links: https://doi.org/10.5281/zenodo.14673608 for systems **A**, **B** and **C**; and https://doi.org/10.5281/zenodo.14675179 for systems **A'**, **B'** and **C'**.

The different reported analysis (Radial distribution functions, density profiles and concentration at the interface) have been performed using our in-house software (MDS). Analysis have been performed over different time intervals to check for convergence (Figure S1-S3). Results reported in the main text have been calculated over the full trajectory (500 ns) and with a time step between two frames of 1 ps, hence every analysis has been done over 500 000 points. Typical snapshots have been performed using the VMD software.

RESULTS AND DISCUSSION

MD study of $[W_5O_{18}Zr(OH)(OH_2)]^{3-}$ ions with TBA^+ counterions in aqueous solution. The Zr-hydroxo-aqua $[W_5O_{18}Zr(OH)(H_2O)]^{3-}$ species (hereinafter referred with the short-hand notation **W_5Zr**) is the active catalytic form proposed in the oxidation of organic substrates[5] and in the hydrolysis of peptide bonds.[7,8] Both processes might involve the presence of dimeric polyoxometalate species with covalent Zr-(μOH)-Zr linkages, in whose formation the anions must approach each other in an appropriate orientation that allows contact distances between the addenda Zr moieties. Previous classical MD studies on a series of non-substituted POMs had shown that these anions can form noncovalent dimers or oligomers in water despite their mutual

coulombic repulsions.[9-11,13] The counterion, solvation and concentration effects allow the two anions to display short-range contacts. For metal-substituted POMs, the number of possible types of noncovalent contacts increases as illustrated in Figure 2. The contacts between two Zr-substituted POMs can be classified as direct and solvent-mediated, and as reactive and unreactive depending whether Zr moieties interact or do not. In the solvent-mediated contacts, the POMs would be connected by bridging H_2O molecules of the aqueous solution as observed in classical MD simulation of $[PW_{12}O_{40}]^{3-}$ and $[SiW_{12}O_{40}]^{4-}$ anions.[12] Simulations on Keggin structures also indicated that hydrophobic forces can induce direct POM···POM contacts,[10] which, however, would be less likely for the smaller Lindqvist-type anions. The replacement of a W=O unit by a Zr moiety generates a total dipole moment in the Zr-substituted POM, and therefore in this case, the direct POM···POM contact could be induced by dipole-dipole interactions. Finally, the direct contacts, in which the Zr moieties of each of the two POMs interact directly, might be driven by hydrogen-bonding involving the aqua and the hydroxo ligands. In this section, we aim to evaluate which of these contacts occurs more frequently in aqueous solution and drives the Zr-substituted POM assembly.

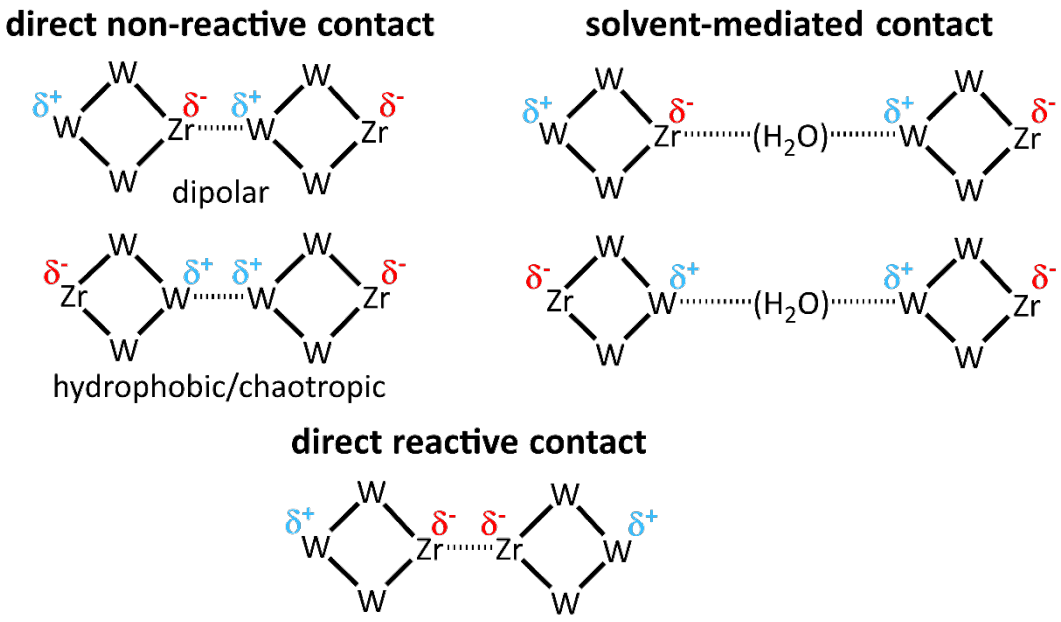

Figure 2. Schematic representation of the possible noncovalent contacts between Zr-monosubstituted POMs.

To study the aggregation of POMs in the bulk, we performed simulations in pure aqueous solutions at three different concentrations, systems **A**, **B** and **C** (see Table 1). Figure 3 shows for each investigated system the snapshots of the system at the end of the simulation together with the radial distribution functions (RDF) calculated over the full productive trajectory between POMs. In the case of the diluted system **A** (0.024 mol·L^{-1}), we observed that POMs sometimes approach each other, but they do not form permanent contacts nor reactive contacts through Zr moieties (Figure S1). This is confirmed by the calculated RDFs between the central oxygen atoms of the POMs (Oc···Oc) and between the Zr atoms (Zr···Zr). The Oc···Oc and Zr···Zr RDFs do not show any clear peak below 11.0 and 6.75 Å, respectively (Figure 3, right). However, when the concentration is increased to 0.068 and 0.178 mol·L^{-1} (systems **B** and **C**, respectively) a peak centered at about 5.70 Å appears in the Zr···Zr RDFs (Figure 3, right), indicating the formation of dimeric adducts with the reactive Zr···Zr orientation. This peak is found to be rather wide pointing to a rather dynamic adduct, while in the most concentrated system **C**, we observe the appearance of an additional peak centered at 5.10 Å. This peak is found to be narrower than that at 5.70 Å pointing to stronger interactions. The exact geometries and dynamics corresponding to these peaks will be discussed further below. In system B the O_c···O_c RDF presents a little shoulder around 10 Å pointing to a tendency for POMs to form close contact adducts, the undefined nature of the shoulder further pointing to the dynamics of these adducts. In system C, additionally to this shoulder around 10 Å which is also present in this system, we observe the appearance of a second clear defined peak at 8.7 Å, further pointing to strong orientated interactions, as already discussed for the peak at 5.1 in Zr-Zr RDFs. The integration values of the RDFs up to 11.0 Å are relatively

low, 0.012 for system **B** and 0.047 for system **C**. To sum up, although the **W_5Zr**···**W_5Zr** contacts are unusual in pure aqueous solution, the directionality of these contacts seems suitable for the subsequent dimerization reaction through Zr moieties.

Additionally, we have analyzed the interaction of **W_5Zr** anions with TBA^+ by determining the RDFs between the central oxygen of **W_5Zr** anion and the nitrogen atom of TBA^+, O_c ···N_{TB}. The RDF plots show a relatively sharp peak centered at about 7.1 Å whose intensity increases with **W_5Zr** concentration (Figure S2). Previous MD simulations of Keggin anions $[PW_{12}O_{40}]^{3-}$ (**PW_{12}**) in aqueous solution revealed that the latter behaved differently in presence of hydrophobic TBA^+ counterions compared to when Cs^+, UO_2^+ or Eu^{3+} were present as counterions.[9] The TBA^+ cations form ion-pairs with **PW_{12}** anions and tend to aggregate into an unstructured domain in the form of a humid molten salt microphase. Consequently, each **PW_{12}** anion is fully surrounded by TBA^+ cations hindering the direct POM···POM contacts. However, in the case of **W_5Zr** anions we did not observe this trend and integration of the first peak (9 Å) showed that on average each **W_5Zr** anion is surrounded by 0.3 (system **A**), 0.62 (system **B**) and 1.12 (system **C**) TBA^+ cations, pointing to the fact that the salt was diluted in the solvent box (see Figure 3). Both **W_5Zr** and **PW_{12}** anions have the same molecular charge (-3) but the Lindqvist-type anion **W_5Zr** is significantly smaller and its negative charge less distributed around the POM framework. Consequently, the **W_5Zr** anion is more hydrophilic than **PW_{12}**, reducing its tendency to form molten salts. In the case of Zr-substituted Keggin anion $[PW_{11}O_{39}Zr(OH)(H_2O)]^{4-}$ (**$PW_{11}Zr$**) the molecular charge (-4) increases with respect to the non-substituted Keggin (-3); and therefore we expect a higher hydrophilic character for the former with a similar behavior to that of Zr-monosubstituted Lindqvist anion.

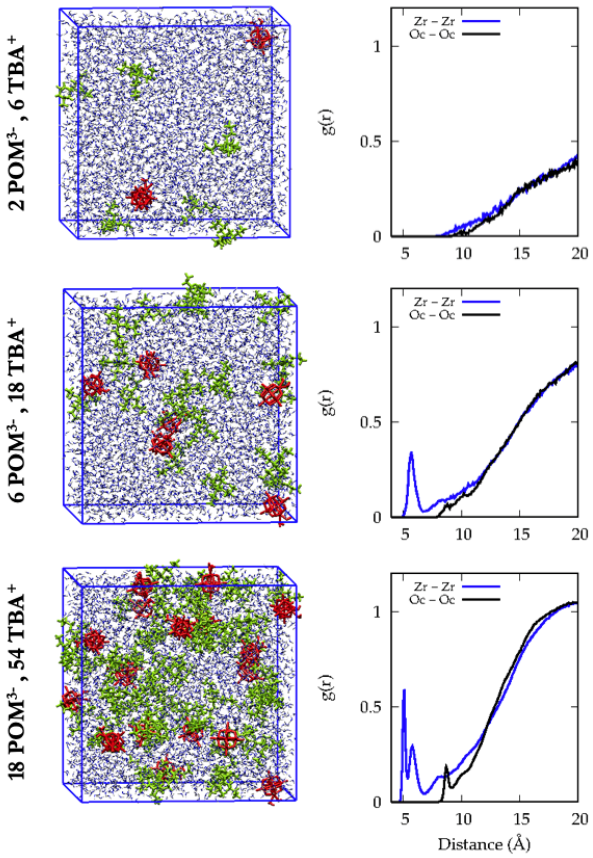

Figure 3. x **W_5Zr**, 3x TBA^+ for x = 2 (system **A**), 6 (system **B**), and 18 (system **C**) in aqueous solution. Snapshot of the simulated systems after 500 ns (left), radial distribution functions (right) between the central oxygens of the POMs (Oc···Oc, black) and between the addenda Zr atoms (Zr···Zr, blue).

MD study of $[W_5O_{18}Zr(OH)(OH_2)]^{3-}$ ions with TBA^+ counterions in a CLF/water biphasic system. Recent MD studies of **PW_{12}** Keggin anions at aqueous interfaces with organic solvents, indicated that in presence of TBA^+ counterions, the **PW_{12}** are highly surface active.[10] The hydrophobic TBA^+ cations concentrate at the interfaces creating a positive charged layer that attracts POMs anions forming loose contact ion pairs. In these simulations, all POMs displayed

PW_{12}···TBA^+···**PW_{12}** contacts at the interface, hence preventing the formation of direct **PW_{12}**···**PW_{12}** interactions.[10] Thus, the surface activity of POMs may either promote processes such as the assembly or prevent them. To examine at molecular level the possible phenomena at the interface, we repeated the study of the previous systems placing them at the chloroform / water interface (systems **A'**, **B'** and **C'** in Table 1). Figure 4 shows the final snapshots after 500 ns of simulations together with the average density curves for the different species in the system. The density profiles reveal a peak of TBA^+ and POMs at the interface. Visual observation of the trajectories revealed that in all cases, the hydrophobic TBA^+ cations tend to accumulate at the interface, where they then attract the negative charged POMs. The population analysis centered at one of the two interfaces in a slab of 24 Å centered at the interface shows that for system **A'** one finds 1.5 ± 0.5 **W_5Zr** and 5.0 ± 0.1 TBA^+, for system **B'** 2.9 ± 0.5 **W_5Zr** and 9.0 ± 0.7 TBA^+, for system **C'** 6.0 ± 0.8 **W_5Zr** and 16.7 ± 1.6 TBA^+. Hence, this clearly indicates that **W_5Zr** anions tend to accumulate at the interface due to the attraction of TBA^+ cations. Furthermore, the ratio between TBA^+ cations and **W_5Zr** anions is found to be about 3, indicating that the interface is neutral. Interestingly, the substituted POMs are adsorbed at TBA^+ layer adopting a preferred orientation with the Zr moiety pointing to the aqueous solution. Comparing the density peak of the central oxygen atom O_c and the Zr atom (red and black curves in Figure 4) revealed that the O_c peak is closer by 0.9 to 1.2 Å to the interface than the Zr peak. It is reasonable to think that the hydrophilic hydroxo and aqua ligands of Zr determine this orientation. Interestingly, this structural pattern is analogous to that found by MD simulations on the interaction of Zr-substituted polyoxometalates with proteins, in which the POM framework interacts electrostatically with positively charged amino acids and the Zr-hydroxo -aqua moiety points towards the bulk water.[7,8,27]

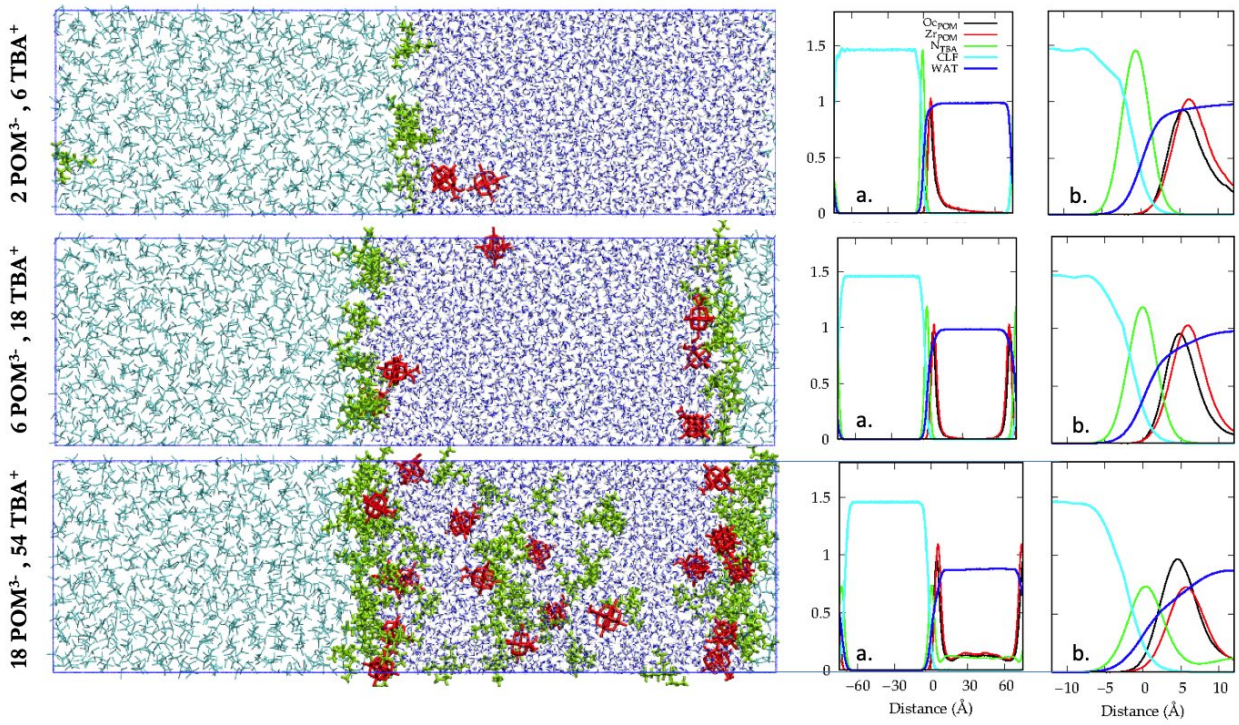

Figure 4. x **W5Zr**, 3x TBA^+ for x = 2 (system **A'**), 6 (system **B'**), and 18 (system **C'**) at the chloroform / water interface. Final snapshot of the simulation (left) and average density curves, over the full simulation box (a) or zoomed in at the interfacial region (b) taken over the last 500 ns of dynamics (right). Chloroform in cyan, water in blue, **O_{cPOM}** in red, Zr_{POM} in black and TBA^+ in green.

We also quantified the amount and efficiency of POM···POM contacts by plotting the RDF plotting in different regions of system **C'** (Figure 5). The O_c···O_c RDFs display a clear sharp peak at about 8.7 Å (black line in Figure 5). Splitting up the contribution to POM in the bulk *vs.* POM at the interface, clearly indicate that this peak results from the contribution of POM at the interface. The integration of overall O_c···O_c RDF (black line) up to a distance of 11 Å in **C'** is about 1.5, while the value of that obtained in pure aqueous system **C** is 0.047. If one only considers POM···POM interactions at the interface of system **C'**, the integration is found to be 0.087 nearly twice that found in pure aqueous system **C**. This trend is even more clearly reflected in the Zr···Zr

RDFs plots. For system **C'**, one can two sharp peaks, one at 5.0 Å (narrow) and one at 5.8 Å (broader), similar to what has been observed for the concentrated aqueous solution **C**. These peaks are far more pronounced when only considering the POMs at the two interfacial regions (red curves), while when only considering POMs in the bulk water region only one broad peak at 5.8 Å is observed (blue curve). Moreover, ongoing from **C** to **C'**, the integration value of Zr···Zr RDF up to a distance of 6.9 Å slightly increases from 0.017 (**C**) to about 0.019 (**C'**). However, when only the interfacial region is considered, this number increases by 60% (0.27). Thus, the local concentration at the interfaces leads to an increase of POM···POM contacts that occur preferentially through the Zr moieties of each POM. This suggest that the driving force for **W_5Zr···W_5Zr** contacts is the Zr-hydroxo and aqua substitution allowing the formation of hydrogen bonds between them.

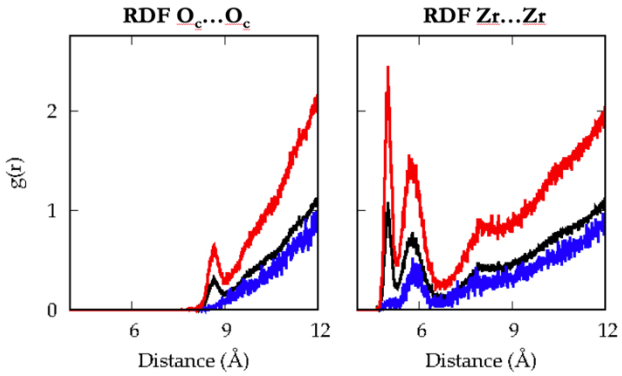

Figure 5. Radial distribution functions (RDFs) for system **C'** between the central oxygens of the POMs (O_c···O_c) and between the addenda Zr atoms (Zr···Zr). Plots computed for all the **W_5Zr** anions of the system (black), for **W_5Zr** at the interfaces (red) and for **W_5Zr** in bulk water (blue).

The O_c···N_{TBA} RDFs for biphasic systems are similar to those of the corresponding pure water one's despite of the local concentration. Recalling the dynamic behavior of **W_5Zr** anions, we can

highlight that they are adsorbed on the TBA^+ layer and not sunken in it, reducing the countercation wrapping. This explains why the local concentration of **W_5Zr** anions does not involve a shielding of the cations that would penalize the formation of direct **W_5Zr**···**W_5Zr** contacts. Thus, the assembly activity at the non-polar/polar domain increases strongly because the reactive **W_5Zr**···**W_5Zr** contacts are more frequent.

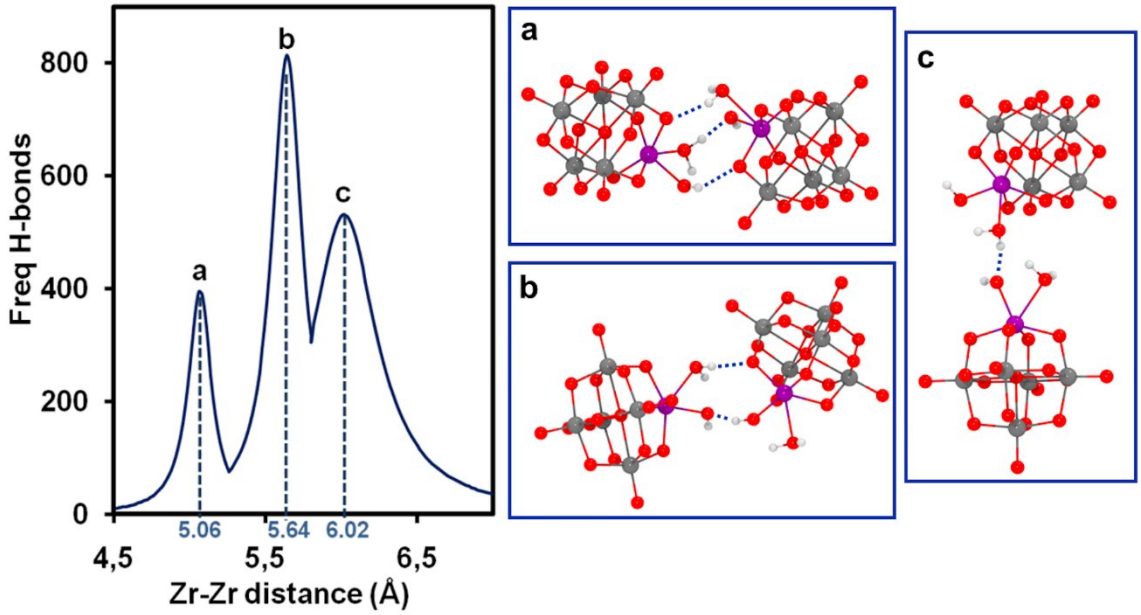

Figure 6. Frequency of the number of hydrogen bonds between two selected **W_5Zr** anions vs. the Zr-Zr distance (left panel), and snapshots of representative dimeric adducts for the peaks **a**, **b** and **c** (right panels).

To analyze in more detail the nature of noncovalent interactions between Zr-substituted POMs in the bulk, we selected a long lifetime reactive **W_5Zr**···**W_5Zr** contact (Zr···Zr distance < 7 Å) in a simulation with 18 **W_5Zr**, 54 TBA^+, 2738 H_2O and 785 CLF (system **C'**). The trajectory lasted for ~1.5 ns, and in it, we could identify several types of intermolecular hydrogen bonds between the two **W_5Zr** anions. Figure 6 displays the frequency of hydrogen bonds as a function of the Zr···Zr distance, as well as, representative snapshots of spontaneously forming noncovalent

dimers, obtained along the selected trajectory. As criterion for hydrogen bond formation, we used a threshold for H···O distance of 2.5 Å. We observed three peaks in the graph at Zr···Zr distances of 5.0, 5.6 and 6.0 Å corresponding respectively to dimeric adducts with three, two and one hydrogen bonds. As expected, the higher the number of hydrogen bonds is, the shorter the Zr···Zr distance. Thus, the stabilization of the **W_5Zr···W_5Zr** adduct with a higher number of hydrogen bonds is counterbalance by the increase of the repulsion between the two **W_5Zr** anions. The highest peak b in the graph corresponds two an intermediate situation, two hydrogen bonds and Zr···Zr distance of 5.6 Å, which might describe the optimal interaction between **W_5Zr** anions. The most frequent hydrogen bonds are: (1) H_w···O_h between an aqua ligand hydrogen and a hydroxo ligand oxygen; (2) H_w···O_b between an aqua ligand hydrogen and a bridging Zr-O-W oxygen; and (3) H_h···O_b between a hydroxo ligand hydrogen and a bridging Zr-O-W oxygen. These Zr···Zr distances at which the hydrogen bond frequency appears to agree well with that of the first peak of the Zr···Zr RDFs in system **C'** (5.8 and 5.95 Å, respectively). As we showed in a previous contribution, these dimeric adducts are similar to those determined at DFT level that connect directly to the transition state for Zr-μO-Zr bond formation.[31] Thus, we can conclude that **W_5Zr**'s activity at the interface favors the formation of reactive dimeric adducts.

Free energy profile for the interactions between W_5Zr···W_5Zr anions in water by Potential Mean Force (PMF) simulations. It would be useful to know how the free-energy changes when two Zr-substitued POMs approach each other in aqueous solution. To assess the free-energy changes when two Zr-substitued POMs approach each other in aqueous solution, we performed Potential of Mean Force (PMF) calculations using the distance between the central oxygens of two **W_5Zr** anions (O_c···O_c) as reaction coordinate. PMF generates a series of configurations along the reaction coordinate and averages the free energy calculated at each step. Thus, the O_c···O_c distance was varied within the interval ranging from 17.5 to 7.5 Å by steps of 0.1 Å for systems **A**, **B** and

C. The results are independent of the starting configuration and free-energy profiles along the POM-POM dimer adduct formation are given in Figure **7**. All the free energy curves reveal a local minimum at a $O_c \cdots O_c$ distance around 8.7 Å, this minimum is somewhat more pronounced in the highly concentrated systems. In all systems the energy cost for bringing the two **W_5Zr** anions together is found to be slightly unfavorable (1-3 kcal.mol^{-1}). This free-energy can however be easily overcome at ambient temperature in agreement with the short noncovalent contacts between monomers observed during MD simulations. Note that PMF simulations have been limited to the simulations in the bulk solution (System A, B and C), as in the case of the biphasic systems (A', B' and C') results would be much more complex to analyze. At the interface, the free-energy change of POM···POM adduct formation could be biased by the intrinsic complexity of the interaction mechanism at the interface. Thus, the dimer formation could occur between two anions at the interface, or between one at the interface and the other initially in the bulk. Also, PMF simulations should ensure that the anions remain at the interface during the free-energy evaluation and consider the impact of the local concentration of **W_5Zr** and TBA^+ countercations at the interface.

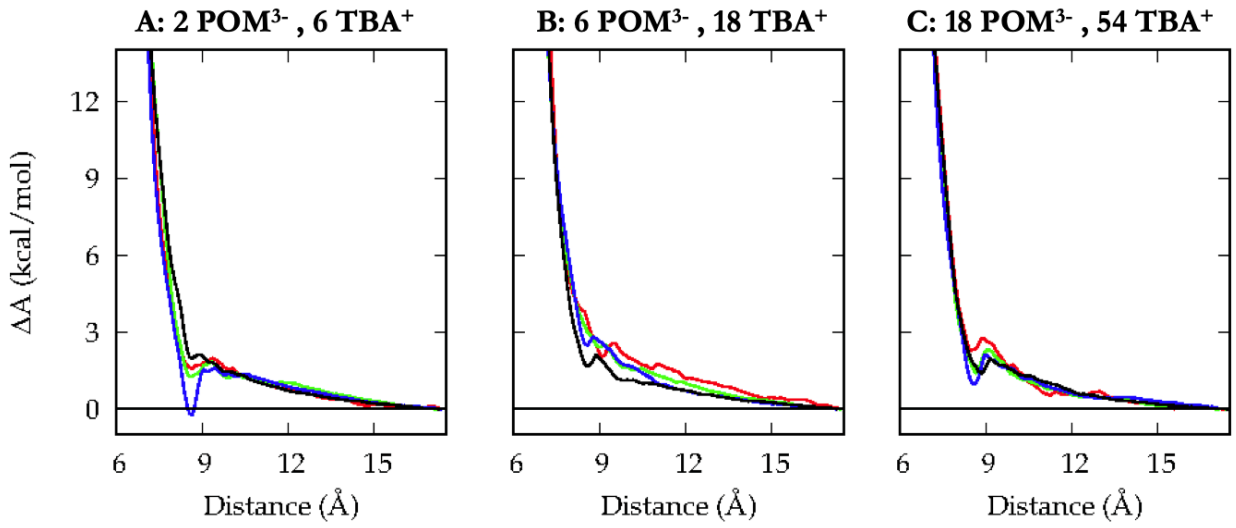

Figure 7. Potential of Mean Force (PMF) simulation of systems x **W_5Zr**, 3x TBA^+ for x = 2 (system **A**), 6 (system **B**), and 18 (system **C**). Helmholtz free energy variation as a function of the $O_c \cdots O_c$ distances starting at 17.5 Å. Sampling time 100 (red), 400 (green), 800 (blue) and 1600 ps (black).

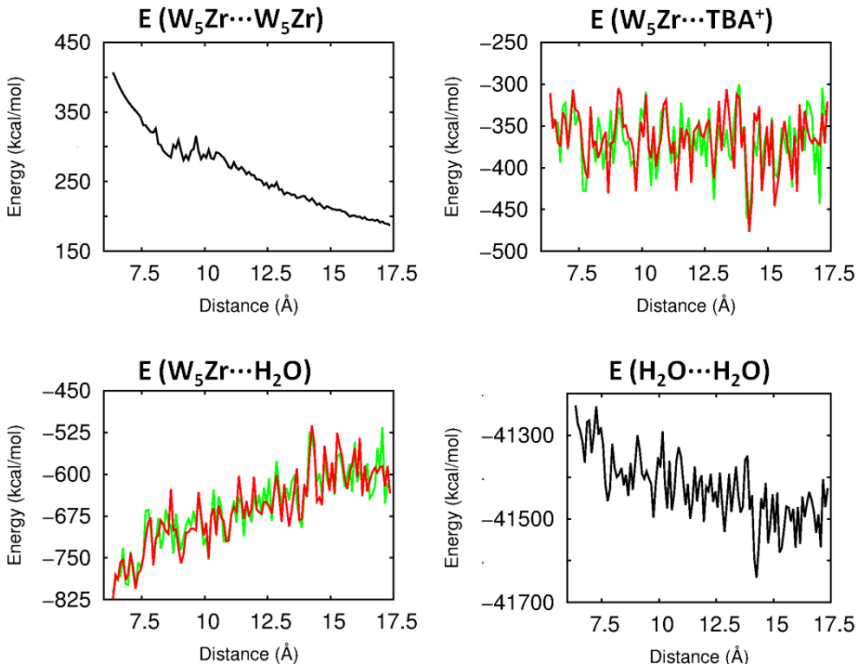

Figure 8. Evolution of the interaction energies components along PMF simulations for system **A** and 1600 ps of sampling time. Energy components in kcal.mol^{-1} as a function of $O_c \cdots O_c$ distance in Å.

We selected the PMF simulation in system **A** with 1600 ps of sampled time in order to analyze the interaction energy between the different species in solution (Figure 8). Upon decreasing the $O_c \cdots O_c$ distance, the repulsion energy between the two **W$_5$Zr** anions increases until it reaches a plateau in the distance range 10.5 – 8.5 Å, and then it continues increasing. The energetic plateau can be rationalized as a favorable region for hydrogen bond formation between POMs that compensates the coulombic repulsion between them. We also observed a gain in solvation energy, E(**W$_5$Zr**$\cdots H_2O$) in Figure 8, that it is the driving force for the formation of long lifetime noncovalent contacts between **W$_5$Zr** anions. It is import to remark that each **W$_5$Zr** anion is better solvated by about 130 kcal.mol^{-1} when the dimeric adduct is formed than when they are isolated. The gain of solvation energy for both **W$_5$Zr** anions is compensated by the loss of intra solvent

energy, E($H_2O\cdots H_2O$) in Figure 8, by 100–120 kcal.mol^{-1}. The solute cavity in the dimer (q = -6) has a larger charge density than in the two separate monomers (q = -3) resulting in proportionally larger solvation energies that are partially compensated by reduction of water···water interactions.

CONCLUSIONS

We have studied the macroscopic aspects involved on the collective behavior of Zr-substituted polyoxometalates (POMs) in solution. Classical MD simulations of $[W_5O_{18}Zr(OH)(H_2O)]^{3-}$ (**W_5Zr**) in the aqueous solution with or without organic interfaces demonstrated that Zr-Lindqvist anions do not form permanent noncovalent contacts. Although in bulk water the **W_5Zr**···**W_5Zr** contacts are unusual, they occur preferentially through Zr moieties; and this directionality is in favor of a covalent assembly. The Zr···Zr contacts are driven by intermolecular hydrogen bonding involving the acidic protons of hydroxo and aqua ligands of Zr. Detailed analysis revealed that noncovalent dimers are present with one, two and up to three hydrogen bonds.

The Zr substitution in the POM structure increases its hydrophylicity, reducing its tendency to form aggregates with hydrophobic TBA^+ counterions. When the biphasic water / chloroform system was simulated, the hydrophobic TBAs accumulate at the interface, creating a positively charged layer that attracts the POM anions. The **W_5Zr** anions lay adsorbed in the TBA layer with hydrophilic Zr-aqua-hydroxo moiety pointing to the aqueous solution. This macroscopic behavior generates a local concentration of **W_5Zr** anions at the interface but without the counteraction wrapping that would shield **W_5Zr**···**W_5Zr** contacts. Thus, the activity of the Zr-substituted POMs increases at the interface favoring the formation of reactive contacts to yield the assembled structures. PMF simulations showed that there is only a short free-energy penalty for bringing two **W_5Zr** together in solution (2 – 3 kcal.mol^{-1}) that can be easily overcome at ambient temperature. Overall, our simulations provided insight into the behavior of Zr-substituted polyoxometalates in

aqueous solution, useful to deeper understanding their performance in catalysis and in assembly processes.

ASSOCIATED CONTENT

Supporting Information. Additional analysis of molecular dynamics simulations are provided in a PDF file.

AUTHOR INFORMATION

Corresponding Author

*Jorge J. Carbó, Departament de Química Física i Inorgànica, Universitat Rovira i Virgili, Tarragona, Spain. E-mail: j.carbo@urv.cat

*Alain Chaumont, Laboratoire MSM, UMR CNRS 7140, Chimie de la Matière Complexe, Université de Strasbourg, 4, rue B. Pascal, 67000 Strasbourg, France. E-mail: chaumont@unistra.fr

Author Contributions

The manuscript was written through contributions of all authors. All authors have given approval to the final version of the manuscript.

ACKNOWLEDGMENT

We thank grant PID2021-128128NB-I00 funded by MICIU/AEI/10.13039/501100011033 and by ERDF/EU and the Generalitat de Catalunya (2021SGR00110).

REFERENCES

1. Pope, M. T. Heteropoly and Isopoly Oxometalates; Springer–Verlag,: New York, 1983.

2. (a) Ni, Z.; Lv, H.; Yang, G., Recent Advances of Ti/Zr substituted Polyoxometalates: From Structural Diversity to Functional Applications. *Molecules*, **2022***, 27,* 8799; (b) Passadis, S. S.;

Gray, M.; Parac-Vogt, T. N.; Keramidas, A. D.; Miras, H. N.; Kabanos, T. A. Revitalisation of group IV metal-oxo clusters: synthetic approaches, structural motifs and applications. *Dalton Trans.* ASAP, DOI: 10.1039/d4dt02417f.

3. (a) Villanneau, R.; Carabineiro, H.; Carrier, X.; Thouvenot, R.; Herson, P.; Lemos, F.; Ramôa Ribeiro, F.; Che, M. Synthesis and Characterization of Zr(IV) Polyoxotungstates as Molecular Analogues of Zirconia-Supported Tungsten Catalysts. *J. Phys. Chem. B* **2004**, *108*, 12465−12471; (b) Carabineiro, H.; Villanneau, R.; Carrier, X.; Herson, P.; Lemos, F.; Ramôa Ribeiro, F.; Proust, A.; Che, M. Zirconium-Substituted Isopolytungstates: Structural Models for Zirconia-Supported Tungsten Catalysts. *Inorg. Chem*. **2006**, *45*, 1915−1923.
4. (a) Kholdeeva, O. A.; Maksimov, G. M.; Maksimovskaya, R. I.; Vanina, M. P.; Trubitsina, T. A.; Naumov, D. Y.; Kolesov, B. A.; Antonova, N. S.; Carbó, J. J.; Poblet, J. M. ZrIV-Monosubstituted Keggin-Type Dimeric Polyoxometalates: Synthesis, Characterization, Catalysis of H_2O_2-Based Oxidations, and Theoretical Study. *Inorg. Chem*. **2006**, *45*, 7224−7234; (b) Kholdeeva, O. A.; Maksimovskaya, R. I. Titanium- and Zirconium-Monosubstituted Polyoxometalates as Molecular Models for Studying Mechanisms of Oxidation Catalysis. *J. Mol. Catal. A: Chem*. **2007**, *262*, 7−24.
5. (a) Maksimchuk, N. V.; Evtushok, V. Y.; Zalomaeva, O. V.; Maksimov, G. M.; Ivanchikova, I. D.; Chesalov, Y. A.; Eltsov, I. V.; Abramov, P. A.; Glazneva, T. S.; Yanshole, V. V.; Kholdeeva, O. A.; Errington, R. J.; Solé-Daura, A.; Poblet, J. M.; Carbó, J. J. Activation of H_2O_2 over Zr(IV). Insights from Model Studies on Zr-Monosubstituted Lindqvist Tungstates. *ACS Catal*. **2021**, *11*, 10589−10603; (b) Maksimchuk, N. V.; Puiggalí-Jou, J.; Zalomaeva, O. V.; Larionov, K. P.; Evtushok, V. Y.; Soshnikov, I. E.; Solé-Daura, A.; Oxana A. Kholdeeva, O. A.; Poblet, Carbó, J. J. Resolving the Mechanism for H_2O_2 Decomposition over Zr(IV)-

Substituted Lindqvist Tungstate: Evidence of Singlet Oxygen Intermediacy. *ACS Catal.* **2023**, *13*, 10324−10339.

6. van Rompuy, L. S., and Parac-Vogt, T. N. Interactions between Polyoxometalates and Biological Systems: from Drug Design to Artificial Enzymes. *Curr. Opin. Biotechnol*. **2019**, *58*, 92–99.
7. Paul, T. J.; Parac-Vogt, T. N.; Quiñonero, D.; Prabhakar, R. Investigating Polyoxometalate-Protein Interactions at Chemically Distinct Binding Sites. *J. Phys. Chem. B*, **2018**, *122*, 7219-7232.
8. Solé-Daura, A.; Rodríguez-Fortea, A.; Poblet, J. M.; Robinson, D.; Hirst, J. D.; Carbó, J. J. Origin of Selectivity in Protein Hydrolysis by Zr(IV)-Containing Metal Oxides as Artificial Proteases. *ACS Catal*. **2020**, *10*, 13455-13467.
9. Chaumont, A.; Wipff, G. Ion Aggregation in Concentrated Aqueous and Methanol Solutions of Polyoxometallates Keggin Anions: the Effect of Counterions Investigated by Molecular Dynamics Simulations. *Phys. Chem. Chem. Phys*. **2008**, *10*, 6940−6953.
10. Chaumont, A.; Wipff, G. Polyoxometalate Keggin Anions at Aqueous Interfaces with Organic Solvents, Ionic Liquids, and Graphite: a Molecular Dynamics Study. *J. Phys. Chem. C*, **2009**, *113*, 18233-18243.
11. Chaumont, A.; Wipff, G. Do Keggin Anions Repulse Each Other in Solution? The Effect of Solvent, Counterions and Ion Representation Investigated by Free Energy (PMF) Simulations. *C. R. Chim*. **2012**, *15*, 107−117.
12. Chaumont, A.; Wipff, G. Interactions Between Keggin Anions in Water: the Higher their Charge, the Higher their Condensation? A Simulation Study. *Eur. J. Inorg. Chem*. **2013**, 1835−1853.

13. Bera, M. K.; Qiao, B.; Seifert, S.; Burton-Pye, B. P.; Olvera de la Cruz, M.; Antonio, M. R. Aggregation of Heteropolyanions in Aqueous Solutions Exhibiting Short-Range Attractions and Long-Range Repulsions. *J. Phys. Chem. C* **2016**, *120*, 1317−1327.

14. Serapian, S. A.; Bo, C. Simulating the Favorable Aggregation of Monolacunary Keggin Anions. *J. Phys. Chem. B* **2016**, *120*, 12959−12971.

15. Mei, Y.; Huang, W.; Yang, Z.; Wang, J.; Yang, X. Ion-Pairing and Aggregation of Ionic Liquid-Neutralized Polyoxometalate Salts in Aqueous Solutions. *Fluid Phase Equilib*. **2016,** *425*, 31−39.

16. Solé-Daura, A.; Notario-Estévez, A.; Carbó, J. J.; Poblet, J. M.; de Graaf, C.; Monakhov, K. Y.; López, X. How Does the Redox State of Polyoxovanadates Influence the Collective Behavior in Solution? A Case Study with $[I@V_{18}O_{42}]^{q-}$ (q = 3, 5, 7, 11, and 13). *Inorg. Chem*. **2019**, *58*, 3881−3894.

17. Segado, M.; Nyman, M.; Bo, C. Aggregation Patterns in Low- and High-Charge Anions Define Opposite Solubility Trends. *J. Phys. Chem. B* **2019**, *123*, 10505−10513.

18. Solé-Daura, A.; Poblet, J. M.; Carbó, J. J. Structure–Activity Relationships for the Affinity of Chaotropic Polyoxometalate Anions towards Proteins. *Chem. Eur. J*. **2020**, *26*, 5799 –5809.

19. Segado-Centellas, M.; Falaise, C.; Leclerc, N.; Priso, G. M.; Haouas, M.; Cadot, E.; Bo C. Nanoconfinement of polyoxometalates in cyclodextrin: computational inspections of the binding affinity and experimental demonstrations of reactivity modulation. *Chem. Sci.* **2024**, *15*, 15849–15857.

20. Schreiber, R. E.; Houben, L.; Wolf, S. G.; Leitus, G.; Lang, Z.-L. Carbó, J. J. Poblet, J. M.; Neumann, R. Real-time molecular scale observation of crystal formation. *Nat. Chem.* **2017**¸ *9*, 369-373.

21. Nikoloudakis, E.; Karikis, K.; Laurans, M.; Kokotidou, C.; Solé-Daura, A.; Carbó, J. J.; Charisiadis, A.; Charalambidis, G.; Izzet, G.; Mitraki, A.; Douvas, A. M.; Poblet, J. M.; Proust, A.; Coutsolelos, A. G. Self-assembly study of nanometric spheres from polyoxometalate-phenylalanine hybrids, an experimental and theoretical approach. *Dalton Trans*., **2018**, *47*, 6304–6313.

22. Assaf, K. I.; Nau, W. M. The Chaotropic Effect as an Assembly Motif in Chemistry. *Angew.Chem. Int. Ed*. **2018**, *57*,13968–13981.

23. See for example: Zhang, G.; Keita, B.; Craescu, C. T.; Miron, S.; de Oliveira, P.; Nadjo, L. Polyoxometalate Binding to Human Serum Albumin: A Thermodynamic and Spectroscopic Approach. *J. Phys. Chem. B* **2007**, *111*, 11253–11259.

24. See for example: Khlifi, S.; Marrot, J.; Haouas, M.; Shepard, W. E.; Falaise, C.; Cadot, E. Chaotropic Effect as an Assembly Motif to Construct Supramolecular Cyclodextrin–Polyoxometalate-Based Frameworks. *J. Am. Chem. Soc*. **2022,** *144*, 4469–4477.

25. See for example: Liu, T.; Diemann, E.; Li, H.; Dress, A. W. M.; Müller, A. Self-assembly in aqueous solution of wheel-shaped Mo_{154} oxide clusters into vesicles. Nature **2003**, *426*, 59–62.

26. (a) López, X.; Miró, P.; Carbó, J. J.; Rodríguez-Fortea, A.; Bo, C.; Poblet, J. M. Current trends in the computational modelling of polyoxometalates. *Theor. Chem. Acc*., **2011**, *128*, 393-404;

(b) López, X.; Carbó, J. J.; Bo, C.; Poblet, J. M. Structure, properties and reactivity of polyoxometalates: a theoretical perspective. *Chem. Soc. Rev*., **2012**, *41*, 7537-7571; (c) Gil, A.; Carbó, J. J. Computational Modelling of the Interactions Between Polyoxometalates and Biological Systems. *Frontiers in Chem.* **2022***, 10*, 876630.

27. Solé-Daura, A.; Goovaerts, V.; Stroobants, K.; Absillis, G.; Jiménez-Lozano, P.; Poblet, J. M.; Hirst, J. D.; Parac-Vogt, T. N.; Carbó, J. J. Probing Polyoxometalate–Protein Interactions Using Molecular Dynamics Simulations. *Chem. Eur. J*. **2016**, *22*, 15280 – 15289.

28. (a) Sciortino, G.; Aureliano, M.; Garribba, E. Rationalizing the Decavanadate(V) and Oxidovanadium(IV) Binding to G-Actin and the Competition with Decaniobate(V) and ATP. *Inorg. Chem*. **2021**, *60*, 334–344; (b) Chaudhary, H.; Iashchishyn, I. A.; Romanova, N. V.; Rambaran, M. A.; Musteikyte, G.; Smirnovas, V.; Holmboe, M.; Ohlin, C. A.; Svedružić, Z. M.; Morozova-Roche, L. APolyoxometalates as Effective Nano-Inhibitors of Amyloid Aggregation of Pro-inflammatory S100A9 Protein Involved in Neurodegenerative Diseases. *ACS Appl. Mater. Inter*. **2021**, 13, 26721–26734.

29. Sap, A.; De Zitter, E.; Van Meervelt, L.; Parac-Vogt, T. N. Structural Characterization of the Complex between Hen Egg-White Lysozyme and Zr^{IV}-Substituted Keggin Polyoxometalate as Artificial Protease. *Chem. Eur. J.* **2015**, *21,* 11692 –11695.

30. Jiménez-Lozano, P.; Carbó, J. J.; Chaumont, A.; Poblet, J. M.; Rodríguez-Fortea, A.; Wipff, G. Nature of Zr-Monosubstituted Monomeric and Dimeric Polyoxometalates in Water Solution at Different pH Conditions: Static Density Functional Theory Calculations and Dynamic Simulations. *Inorg. Chem*. **2014**, *53*, 778−786.

31. Jiménez-Lozano, P.; Sole-Daura, A.; Wipff, G.; Poblet, J. M.; Chaumont, A.; Carbo, J. J. Assembly Mechanism of Zr-Containing and Other TM-Containing Polyoxometalates. *Inorg. Chem*. **2017**, *56,* 4148−4156.

32. Villanneau, R.; Carabineiro, H.; Carrier, X.; Thouvenot, R.; Herson, P.; Lemos, F.; Ramôa-Ribeiro, F.; Che, M. Synthesis and Characterization of Zr(IV) Polyoxotungstates as Molecular Analogues of Zirconia-Supported Tungsten Catalysts. *J. Phys. Chem. B* **2004**, *108*, 12465.

33. AMBER : Case, D. A.; Darden, T. A.; Cheatham, T. E.; Simmerling, C. L.; Wang, J.; Duke, R. E.; Luo, R.; Crowley, R.; Walker, R. C. Zhang, W.; Merz, K. M.; Wang, B.; Hayik, S.; Roitberg, A.; Seabra, G.; Kolossvary, I.; Wong, K. F.; Paesani, F.; Vanicek, J.; Wu, X.; Brozell, S. R.; Steinbrecher, T.; Gohlke, H.; Yang, L.; Tan, C.; Mongan, J.; Hornak, V.; Cui, G.; Seetin, M. G.; Sagui, C.; Babin, V.; Kollman, P. A., University of California, San Francisco, 2008.

34. (a) López, X.; Nieto-Draghi, C.; Bo, C.; Bonet-Avalos, J.; Poblet, J. M. J. Polyoxometalates in Solution: Molecular Dynamics Simulations on the α-$PW_{12}O_{40}^{3-}$ Keggin Anion in Aqueous Media. *J. Phys. Chem. A* **2005**, *109*, 1216-1222; (b) Leroy, F.; Miró, P.; Poblet, J. M.; Bo, C.; Bonet-Ávalos, J. Keggin Polyoxoanions in Aqueous Solution: Ion Pairing and Its Effect on Dynamic Properties by Molecular Dynamics Simulations *J. Phys. Chem. B*, **2008**, *112*, 8591-8599.

35. Rappé, A. K.; Casewit, C. J.; Colwell, K. S.; Goddard, W. A., III; Skifff, W. M. J. UFF, a full periodic table force field for molecular mechanics and molecular dynamics simulations. *J. Am. Chem. Soc*. **1992**, *114*, 10024-11035.

36. Jorgensen, W. L.; Maxwell, D. S.; Tirado-Rives, J. Development and Testing of the OPLS All-Atom Force Field on Conformational Energetics and Properties of Organic Liquids *J. Am. Chem. Soc*. **1996**, *118*, 11225-11236.

37. Jorgensen, W. L.; Chandrasekhar, J.; Madura, J. D.; Impey, R. W.; Klein, M. L. Comparison of simple potential functions for simulating liquid water. *J. Chem. Phys*. **1983**, *79*, 926-935.

38. Chang, T.-M.; Dang, L. X.; Peterson, K. A. Computer Simulation of Chloroform with a Polarizable Potential Model. *J. Phys. Chem. B* **1997**, *101*, 3413–3419.

39. Darden, T.; York, D.; Pedersen, L. Particle mesh Ewald: An N·log(N) method for Ewald sums in large systems. *J. Chem. Phys*. **1993**, *98*, 10089-10092.

40. Berendsen, H. J. C.; Postma, J. P. M.; van Gunsteren, W. F.; DiNola, A.; Haak, J. R. Molecular dynamics with coupling to an external bath. *J. Chem. Phys*. **1984**, *81*, 3684 –3690.

41. Swope, W. C.; Andersen, H. C.; Berens, P. H.; Wilson, K. R. A computer simulation method for the calculation of equilibrium constants for the formation of physical clusters of molecules: Application to small water clusters. *J. Chem. Phys*. **1982**, *76*, 637-649.

Table of Contents.

The collective behavior of Zr-substituted polyoxometalates (POMs) in aqueous solution has been analyzed through molecular dynamics simulations. The Zr-hydroxo-aqua $[W_5O_{18}Zr(OH)(H_2O)]^{3-}$ anions do not form permanent contacts, but the interaction is directional occurring preferentially through hydrogen-bonding between the Zr moieties, whose free-energy was evaluated via potential of mean force (PMF) simulations. In biphasic systems, the TBA^+ countercations accumulate at the organic interface and attract POM anions, increasing their local concentration, and promoting the active POM···POM contacts.